

# Unfolded Protein Response in Cancer: IRE1 $\alpha$ Inhibition by Selective Kinase Ligands Does Not Impair Tumor Cell Viability

Paul E. Harrington,<sup>\*,†</sup> Kaustav Biswas,<sup>\*,†</sup> David Malwitz,<sup>†,‡</sup> Andrew S. Tasker,<sup>†</sup> Christopher Mohr,<sup>‡</sup> Kristin L. Andrews,<sup>‡</sup> Ken Dellamaggiore,<sup>§</sup> Richard Kendall,<sup>§</sup> Holger Beckmann,<sup>||</sup> Peter Jaeckel,<sup>||</sup> Silvia Materna-Reichert,<sup>||</sup> Jennifer R. Allen,<sup>†</sup> and J. Russell Lipford<sup>§</sup>

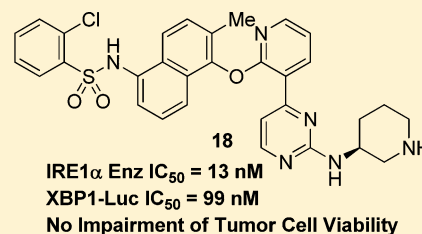
<sup>†</sup>Departments of Medicinal Chemistry, <sup>‡</sup>Molecular Structure, and <sup>§</sup>Oncology, Amgen, Inc., One Amgen Center Drive, Thousand Oaks, California 93012, United States

<sup>||</sup>Department of Discovery Technologies, Amgen Research GmbH, Josef-Engert-Str. 11, 93050 Regensburg, Germany

## S Supporting Information

**ABSTRACT:** The kinase/endonuclease inositol requiring enzyme 1 (IRE1 $\alpha$ ), one of the sensors of unfolded protein accumulation in the endoplasmic reticulum that triggers the unfolded protein response (UPR), has been investigated as an anticancer target. We identified potent allosteric inhibitors of IRE1 $\alpha$  endonuclease activity that bound to the kinase site on the enzyme. Structure–activity relationship (SAR) studies led to **16** and **18**, which were selective in kinase screens and were potent against recombinant IRE1 $\alpha$  endonuclease as well as cellular IRE1 $\alpha$ . The first X-ray crystal structure of a kinase inhibitor (**16**) bound to hIRE1 $\alpha$  was obtained. Screening of native tumor cell lines (>300) against selective IRE1 $\alpha$  inhibitors failed to demonstrate any effect on cellular viability. These results suggest that IRE1 $\alpha$  activity is not essential for viability in most tumor cell lines, in vitro, and that interfering with the survival functions of the UPR may not be an effective strategy to block tumorigenesis.

**KEYWORDS:** Unfolded protein response, IRE1 $\alpha$ , kinase, inhibitor



Cells respond to accumulation of unfolded proteins in the endoplasmic reticulum (ER) by activating a cascade known as the unfolded protein response (UPR) to maintain protein synthesis homeostasis.<sup>1</sup> There are three branches of the UPR involving three transmembrane sensor proteins, PERK, IRE1 $\alpha$ , and ATF6, of which IRE1 $\alpha$  (inositol requiring enzyme 1 $\alpha$ ) is the most conserved branch of the three. It is a transmembrane, bifunctional protein with kinase and endonuclease activity. The N-terminal domain of IRE1 $\alpha$  is proposed to sense the presence of unfolded proteins in the ER lumen, triggering autophosphorylation and dimerization/oligomerization, which, in turn, activates the C-terminal endonuclease. This activity results in the specific excision of 26 nucleotides from the mRNA of the primary UPR transcription factor, XBP1, which is then religated to form spliced XBP1s, whose target genes permit the ER to adapt to stress.<sup>2</sup>

Activation of the UPR has been shown to be an important survival pathway for tumors of secretory cell origin like multiple myeloma that have a very high protein synthesis burden. Therefore, efforts to inhibit the UPR stress response by blocking the IRE1 $\alpha$  endonuclease cleavage and activation of XBP1 has been an active area of cancer research. A potent and selective IRE1 $\alpha$  inhibitor would serve as an important tool to test the hypothesis that, without UPR activation, tumor cells would be driven to apoptosis. In an effort to probe this pathway and identify suitable preclinical leads, we examined potential IRE1 $\alpha$  benchmarks from publications.<sup>3–7</sup> However, a survey of

the literature available at the time<sup>3</sup> suggested that potency and/or selectivity were suboptimal in published compounds. Therefore, we initiated a high throughput screen (HTS) of the Amgen small molecule collection and subsequent hit-to-lead optimization by structure–activity relationship (SAR) studies. Our investigations led to the identification of **16** and **18**, which were examined as chemical tools for probing the role of IRE1 $\alpha$  in cancer cells. In this letter, we report the SAR optimization campaign from our initial hit, the first crystal structure of a kinase-inhibitor bound to human IRE1 $\alpha$  enzyme, and the surprising conclusion that inhibition of IRE1 $\alpha$  activity and XBP1s production had minimal effects on the viability of >300 tumor cell lines. This result raises important questions about the therapeutic utility of IRE1 $\alpha$  inhibition as a strategy to target cancer cell growth.

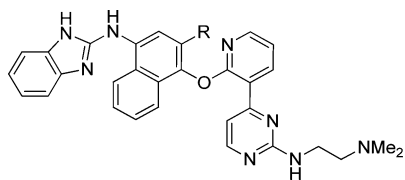
As part of the effort to identify selective inhibitors of IRE1 $\alpha$ , benzimidazole **1** was identified through an HTS campaign (Table 1). Inhibition of IRE1 $\alpha$  RNase activity was determined in an enzyme assay that measured cleavage of the XBP1 stem loop by autophosphorylated IRE1 $\alpha$ . This assay format was chosen to ensure that inhibitors of either the IRE1 $\alpha$  kinase or the RNase domains would be identified. Binding to the ATP

**Special Issue:** New Frontiers in Kinases

**Received:** July 31, 2014

**Accepted:** September 24, 2014

**Published:** September 24, 2014

Table 1. Naphthyl Modification Improves Selectivity<sup>a</sup>

Cpd	R	IRE1 $\alpha$ Enz IC <sub>50</sub> ( $\mu$ M)	XBP1-Luc IC <sub>50</sub> ( $\mu$ M)	Aurora p-histone H3 IC <sub>50</sub> ( $\mu$ M)	JNK3 Enz IC <sub>50</sub> ( $\mu$ M) <sup>b</sup> (fold) <sup>c</sup>
1	H	0.071	0.27	16	0.35 (4.9)
2	Me	0.014	0.20	>50 <sup>b</sup>	0.71 (51)

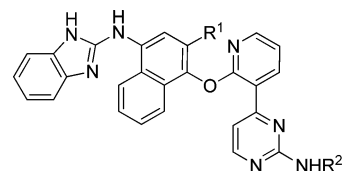
<sup>a</sup>Unless noted otherwise, data represent an average of  $\geq 2$  separate determinations. <sup>b</sup>Data represent a single determination. <sup>c</sup>Fold selectivity versus IRE1 $\alpha$  enzyme.

pocket and inhibition of IRE1 $\alpha$  kinase activity are not required to inhibit the RNase activity. Compounds were also profiled in cellular assays by direct measurement of XBP1s (B-DNA assay) or by quantification of the luciferase signal in HT1080 XBP1-Luc, which carries a luciferase fusion that is only in frame and expressed from the spliced XBP1 transcript. Thapsigargin<sup>8</sup> was used to induce the UPR, activate IRE1 $\alpha$ , and drive splicing of XBP1 or XBP1-luciferase into the proper frame. In the IRE1 $\alpha$  enzyme and XBP1-Luc assays, **1** demonstrated moderate potency and was profiled in a panel<sup>9</sup> of 442 kinases at 1  $\mu$ M to determine broad kinase selectivity. Compound **1** inhibited 17 of 442 kinases at percent of control (POC) < 35. Several of these kinases, including Jun kinases and Aurora kinases, might confound efforts to validate IRE1 $\alpha$  as a target for oncology. Therefore, IC<sub>50</sub> values were determined and are reported for selected kinases in Table 1.

The majority of the hits were recognized kinase inhibitors, even though the screen was designed to identify inhibitors of the IRE1 $\alpha$  RNase activity irrespective of their ability to inhibit the kinase activity. Similar to previous findings,<sup>5</sup> the relative potencies of inhibitors in the kinase assay and RNase assay did not correlate, so we relied on the RNase assay for our SAR efforts. We did identify HTS hits that were not inhibitors of the kinase domain. They bore structural similarity to published IRE1 $\alpha$  inhibitors.<sup>3,4,7</sup> Further mechanistic inspections using mass spectroscopy revealed promiscuous reactivity with both human and yeast IRE1 $\alpha$  enzymes as well as with plasma proteins. These compounds were therefore deemed unsuitable for target validation studies.

Previous work on structurally similar analogues from our Tie-2 program<sup>10</sup> suggested that introducing a methyl group ortho to the ether linkage might improve selectivity against the Aurora kinases. Methyl analogue **2** exhibited improved selectivity against Aurora as measured in the p-Histone H3 cellular assay,<sup>11</sup> while potency in the XBP1-Luc cellular assay was maintained. In addition, selectivity against JNK3 increased from 4.9-fold to 51-fold.

A parallel effort to examine structural modifications of the amine side-chain in **1** provided significant gains in potency (Table 2). The importance of the basic nitrogen for inhibition of IRE1 $\alpha$  was established with **3**. The reduced potency of **4** relative to **1** suggested that a hydroxy group would not be a competent surrogate for a basic nitrogen. Racemic methylpiperidine **5** was nearly equipotent to **1** albeit less selective against JNK3. In the IRE1 $\alpha$  enzyme assay, the *S* enantiomer of des-methylpiperidine **7** was 5-fold more potent than the *R* enantiomer **6** and 7-fold more potent than the HTS hit **1**. The

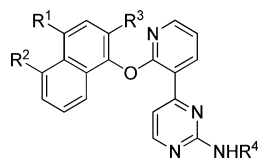
Table 2. SAR of Side-Chain<sup>a</sup>

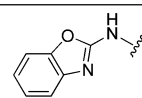
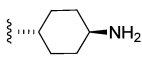
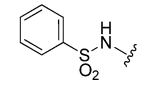
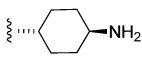
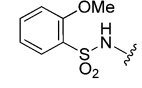
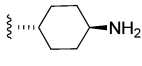
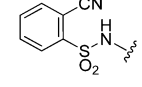
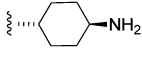
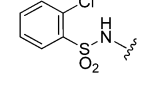
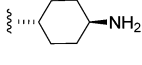
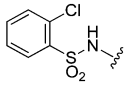
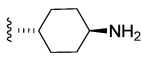
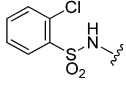
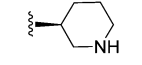
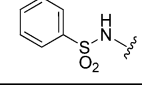
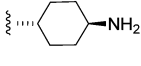
Cpd	R <sup>1</sup>	R <sup>2</sup>	IRE1 $\alpha$ Enz IC <sub>50</sub> ( $\mu$ M)	XBP1 -Luc IC <sub>50</sub> ( $\mu$ M)	JNK3 Enz IC <sub>50</sub> ( $\mu$ M) <sup>b</sup> (Fold) <sup>c</sup>
<b>3</b>	H		>99 <sup>b</sup>	15	0.032 (<0.003)
<b>4</b>	H		0.17	0.87	0.012 (0.071)
<b>5</b>	H		0.029	0.31	0.0055 (0.19)
<b>6</b>	H		0.051	0.57	0.014 (0.27)
<b>7</b>	H		0.0097	0.031	0.031 (3.2)
<b>8</b>	H		0.011	0.033	0.0019 (0.17)
<b>9</b>	H		0.043	0.34	0.0075 (0.17)
<b>10</b>	Me		0.0064	0.033	0.0019 (0.30)
<b>11</b>	Me		0.0051	0.013	0.020 <sup>d</sup> (3.9)

<sup>a</sup>Unless noted otherwise, data represent an average of  $\geq 2$  separate determinations. <sup>b</sup>Data represent a single determination. <sup>c</sup>Fold selectivity versus IRE1 $\alpha$  enzyme.

*trans*-cyclohexanediamine **8** provided a second side-chain with improved potency relative to **1** although *cis*-isomer **9** was 4-fold less active than **8** in the IRE1 $\alpha$  enzyme assay. The *trans*-cyclohexanediamine and (*S*)-3-aminopiperidine were selected as the two side-chains to combine with the methyl naphthyl moiety, thus yielding **10** and **11**, respectively. Although **10** and **11** were potent inhibitors of IRE1 $\alpha$  in both the IRE1 $\alpha$  enzyme and XBP1-Luc cellular assays, we sought to improve the selectivity over JNK3. As part of an effort to examine broad changes to the scaffold, we examined modifications to the benzimidazole. Replacing the benzimidazole with a benzoxazole did not have a significant impact on potency or JNK3 selectivity (**10** vs **12**, Table 3). Sulfonamide **13** emerged as a promising lead to increase selectivity. Despite the 7-fold loss in IRE1 $\alpha$  potency relative to **10**, the JNK3 selectivity increased significantly from 0.3-fold to 49-fold. Substitution at the *ortho* position with an electron donating methoxy functionality (**14**) had minimal influence on potency and selectivity relative to **13**. The electron withdrawing nitrile (**15**) and chloro moieties (**16**) provided gains in IRE1 $\alpha$  enzyme and XBP1-Luc cellular activity.

Sulfonamide **16** was 114-fold selective against JNK3 and was assessed in a panel<sup>9</sup> of 100 kinases in a competition binding assay format. Only five kinases had POC < 30 at 1  $\mu$ M, and

Table 3. Replacement of the Benzimidazole<sup>a</sup>


Cpd	R <sup>1</sup>	R <sup>2</sup>	R <sup>3</sup>	R <sup>4</sup>	IRE1 $\alpha$ Enz IC <sub>50</sub> ( $\mu$ M) <sup>a</sup>	XBP1-Luc IC <sub>50</sub> ( $\mu$ M)	JNK3 Enz IC <sub>50</sub> ( $\mu$ M) (Fold) <sup>c</sup>
12		H	Me		0.014	0.051	0.007 (0.5)
13		H	Me		0.045	0.59	2.2 (49)
14		H	Me		0.054	0.44	1.2 (22)
15		H	Me		0.012	0.062	0.40 (33)
16		H	Me		0.014	0.042	1.6 <sup>b</sup> (114)
17	H		Me		0.022	0.12	0.54 (25)
18	H		Me		0.013	0.099	2.5 (192)
19		H	H		0.031	0.58 <sup>b</sup>	0.40 <sup>b</sup> (13)

<sup>a</sup>Unless noted otherwise, data represent an average of  $\geq 2$  separate determinations. <sup>b</sup>Data represent a single determination. <sup>c</sup>Fold selectivity versus IRE1 $\alpha$  enzyme.

none were anticipated to interfere with validation studies with an IRE1 $\alpha$  inhibitor.<sup>12</sup>

After significant effort, a 2.5 Å X-ray cocrystal structure of **16** bound to dephosphorylated human IRE1 $\alpha$  was obtained (Figure 1). In this structure, the salt bridge between Lys599 and Glu612 is broken, and the *ortho*-chlorophenyl ring occupies the  $\alpha$ C-helix pocket. Tyr628 and the  $\alpha$ C-helix adopt a similar conformation as observed in the yeast crystal structure.<sup>13,14</sup> We did observe a  $\sim 2$  Å shift of the  $\alpha$ C-helix relative to activator bound structures, which along with movement of Leu616 and Glu612, opened the  $\alpha$ C-helix pocket for inhibitor binding. The proximity of the sulfonamide to Lys599 (3.1 Å) suggested it was deprotonated in the bound state. Each of the sulfonamide oxygens formed a hydrogen bond to the backbone NH of Asp711 and Phe712 residues of the DFG motif.

In contrast to previously published IRE1 $\alpha$  structures (e.g., hIRE1 $\alpha$  bound to ADP; PDB code 3P23),<sup>15</sup> we did not observe either a face-to-face or a back-to-back dimer formation with the inhibitor-bound structure. Furthermore, the previous hIRE1 $\alpha$  structure exhibited a shifted and partially disordered  $\alpha$ C-helix, while our structure does not. The lack of dimer/oligomer formation in this instance might be indicative of the inhibitory mechanism of these compounds, as it has been suggested that

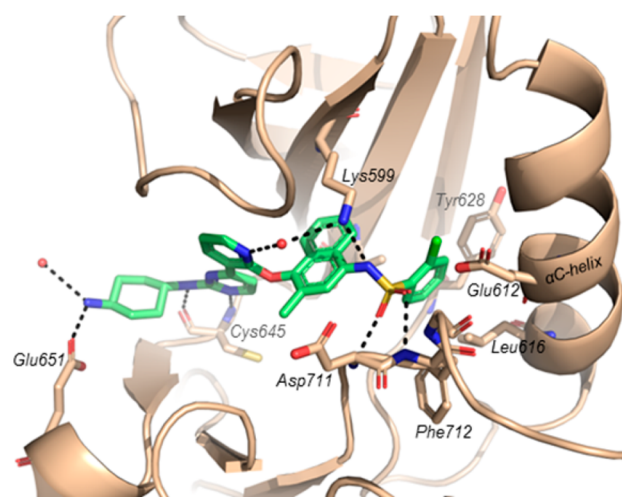
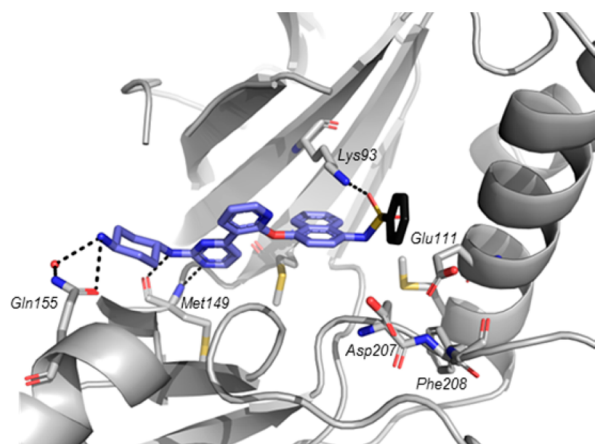


Figure 1. X-ray cocrystal structure of **16** bound to dephosphorylated human IRE1 $\alpha$  (PDB code 4U6R).

oligomerization follows autophosphorylation<sup>14</sup> and subsequent activation of the RNase domain and XBP1 splicing. We

hypothesize that the improved JNK3 selectivity of **16** could be attributed to the inhibitor accessing the  $\alpha$ C-helix pocket in IRE1 $\alpha$ , while this binding mode may be less accessible in JNK3. This is supported by the cocrystal structure of related sulfonamide **19**, which lacks the methyl group in the central naphthyl ring, with JNK3 (Figure 2). In this structure, the



**Figure 2.** X-ray cocrystal structure of **19** bound to JNK3 (PDB code 4U79).

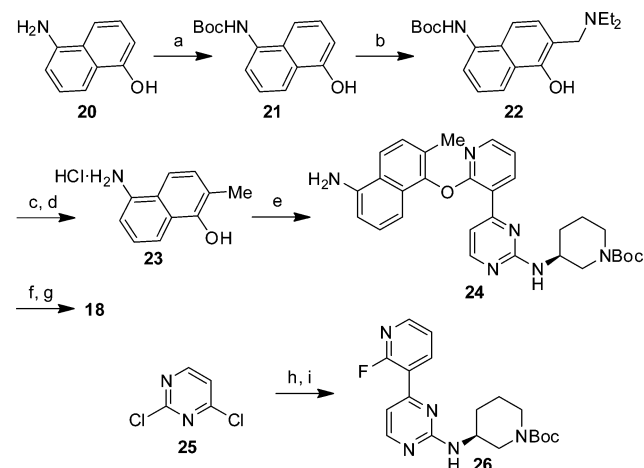
sulfonamide is inverted compared to the IRE1 $\alpha$  cocrystal structure with **16** and, as a result, does not make any favorable interactions with the DFG motif. Additionally, the phenyl group is disordered, oriented toward solvent, and not engaging in any favorable van der Waals contacts.

In addition, from a structure-based design perspective, the structure of **16** bound to human IRE1 $\alpha$  suggested that the sulfonamide group could be transposed from a 1,4-aminonaphthyl to a 1,5-aminonaphthyl and retain activity. This modification yielded sulfonamide **17**, which had IRE1 $\alpha$  potency and JNK3 selectivity similar to **16**. An improvement in IRE1 $\alpha$  potency and JNK3 selectivity was realized by replacing the *trans*-cyclohexanediamine side-chain with (*S*)-3-aminopiperidine yielding **18**. The kinase selectivity of **18** was improved relative to **16**; of the 100 kinases that were examined in a competition binding assay,<sup>9</sup> none had POC < 50 at 1  $\mu$ M.

The synthesis of **18** is shown in Scheme 1. Aminonaphthyl **20** was protected as the Boc carbamate. The methyl group was introduced in a two-step sequence. Mannich condensation of **21** with diethylamine and formaldehyde gave **22** in 74% yield. Reduction of the benzylic C–N in **22** with hydrogen and palladium on carbon provided **23** in 73% yield. A  $S_NAr$  alkylation of **23** with fluoropyridine **26** was used to form the C–O bond in **24**. Reaction of **24** with 2-chlorobenzene-1-sulfonyl chloride followed by deprotection yielded **18**. Fluoropyridine **26** was prepared in two steps from 2,4-dichloropyrimidine by Suzuki–Miyaura cross-coupling followed by chloro displacement with (*S*)-*tert*-butyl 3-aminopiperidine-1-carboxylate.

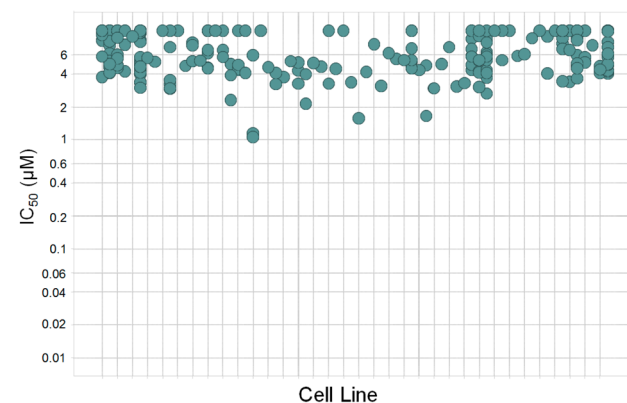
Given the excellent potency and selectivity of **18** and **16**, these compounds were chosen to test the effects of IRE1 $\alpha$  inhibition on the viability of tumor cells. Compound **16** was tested in >200 cell lines (Eurofins) with 3-fold dose response starting at 50  $\mu$ M and failed to demonstrate potent inhibition of cellular viability (Figure 3a). In addition, **18** and/or **16** were tested in similar viability assays on an internal panel of >140 tumor cell lines.<sup>16,17</sup> This panel included 15 multiple myeloma

### Scheme 1. Synthesis of **18**<sup>a</sup>



<sup>a</sup>Reagents and conditions: (a) Boc<sub>2</sub>O, dioxane, 60 °C, 83% yield; (b) Et<sub>2</sub>NH, formaldehyde, MeOH/H<sub>2</sub>O, rt, 74% yield; (c) Pd/C, H<sub>2</sub>, EtOH, rt, 73% yield; (d) HCl, DCM, 35 °C, quantitative; (e) **26**, Cs<sub>2</sub>CO<sub>3</sub>, NMP, 120 °C, 69% yield; (f) 2-chlorobenzene-1-sulfonyl chloride, pyridine, rt, 95% yield; (g) TFA, DCM, rt, 92% yield; (h) (2-fluoropyridin-3-yl)boronic acid, Pd(PPh<sub>3</sub>)<sub>4</sub>, K<sub>2</sub>CO<sub>3</sub>, dioxane/H<sub>2</sub>O, 90 °C, 60% yield; (i) (*S*)-*tert*-butyl 3-aminopiperidine-1-carboxylate, Et<sub>3</sub>N, DMSO, 100 °C, 52% yield.

### (a) Viability of >200 Tumor Cell Lines



### (b) Viability of the multiple myeloma cell line NCI-H929-Luc

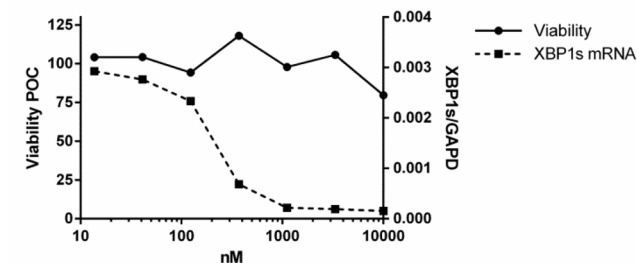


**Figure 3.** Inhibition of IRE1 $\alpha$  does not impact viability of tumor cell lines, despite near-complete reduction of XBP1s. (a) Compound **16** was tested in a viability assay (nuclear count) in >200 tumor cell lines (Eurofins OncoPanel 240). The IC<sub>50</sub> IP for viability is represented on the y-axis, and each tumor cell line tested is listed on the x-axis. (b) Viability of the multiple myeloma cell line, NCI-H929-Luc, was determined by ATPlite after 48 h of treatment with **18**. POC was calculated as percent of DMSO control at 48 h. XBP1s and GAPD mRNA levels were quantified by bDNA after 2 h of treatment with **18**.

cell lines with high levels of IRE1 $\alpha$  activity as measured by elevated baseline levels of XBP1s. Despite robust inhibition of XBP1s (measured in a subset of lines), none of the cell lines that were examined demonstrated sensitivity to inhibition of IRE1 $\alpha$  by **18** or **16** (Figure 3b). These results are surprising given our expectation of the key role of IRE1 $\alpha$  and UPR in maintaining the viability of cancer cells with high protein synthesis load (e.g., multiple myeloma) and suggest that IRE1 $\alpha$  does not play a critical role in tumor cell survival, at least in cell culture.<sup>18</sup>

In summary, an effort to improve the potency of the HTS lead **1** (IRE1 $\alpha$  Enz IC<sub>50</sub> = 0.071  $\mu$ M and XBP1 IC<sub>50</sub> = 0.27  $\mu$ M) resulted in sulfonamide **18** (IRE1 $\alpha$  Enz IC<sub>50</sub> = 0.013  $\mu$ M and XBP1 IC<sub>50</sub> = 0.099  $\mu$ M). The JNK3 selectivity was improved from 4.9-fold (**1**) to 192-fold (**18**), respectively. Modification of the naphthyl and basic side-chain resulted in increased IRE1 $\alpha$  potency and JNK3 selectivity. The X-ray cocrystal structure of **16** bound to human IRE1 $\alpha$  provided insight for further optimization to **18**. In panels of >300 tumor cell lines, **16** and **18** did not significantly impair cellular viability. These results suggest that selective inhibition of IRE1 $\alpha$  may not lead to reduced tumorigenesis and suggests a re-evaluation of this bifunctional kinase-RNase as a target for anticancer therapeutic development.

## ■ ASSOCIATED CONTENT

### Ⓢ Supporting Information

In vitro assay protocols, X-ray crystallographic data, Eurofins OncoPanel data, kinase selectivity data for **1**, **16**, and **18**, synthetic experimental procedures for **18**, and characterization data for compounds **1**–**19**. This material is available free of charge via the Internet at <http://pubs.acs.org>.

## ■ AUTHOR INFORMATION

### Corresponding Authors

\*(P.E.H.) E-mail: [pharring@amgen.com](mailto:pharring@amgen.com).

\*(K.B.) E-mail: [kbiswas@amgen.com](mailto:kbiswas@amgen.com).

### Present Address

<sup>†</sup>Janssen Research and Development, LLC., 3210 Merryfield Row, San Diego, California 92121, United States.

### Author Contributions

The manuscript was written through contributions of all authors. All authors have given approval to the final version of the manuscript.

### Notes

The authors declare no competing financial interest.

## ■ ACKNOWLEDGMENTS

We thank Dr. Iain Campuzano for the acquisition of high-resolution mass spectra.

## ■ REFERENCES

- (1) Walter, P.; Ron, D. The Unfolded Protein Response: From Stress Pathway to Homeostatic Regulation. *Science* **2011**, *334*, 1081–1086.
- (2) Chen, Y.; Brandizzi, F. IRE1: ER stress sensor and cell fate executor. *Trends Cell Biol.* **2013**, *23*, 547–555.
- (3) Volkmann, K.; Lucas, J. L.; Vuga, D.; Wang, X.; Brumm, D.; Stiles, C.; Kriebel, D.; Der-Sarkissian, A.; Krishnan, K.; Schweitzer, C.; Liu, Z.; Malyankar, U. M.; Chiovitti, D.; Canny, M.; Durocher, D.; Sicheri, F.; Patterson, J. B. Potent and selective inhibitors of the inositol-requiring enzyme 1 endoribonuclease. *J. Biol. Chem.* **2011**, *286*, 12743–12755.

- (4) Cross, B. C. S.; Bond, P. J.; Sadowski, P. G.; Jha, B. K.; Zak, J.; Goodman, J. M.; Silverman, R. H.; Neubert, T. A.; Baxendale, I. R.; Ron, D.; Harding, H. P. The molecular basis for selective inhibition of unconventional mRNA splicing by an IRE1-binding small molecule. *Proc. Natl. Acad. Sci. U.S.A.* **2012**, *109*, E869–E878.

- (5) Wang, L.; Perera, B. G. K.; Hari, S. B.; Bhatarani, B.; Backes, B. J.; Seeliger, M. A.; Schurer, S. C.; Oakes, S. O.; Papa, F. R.; Maly, D. J. Divergent allosteric control of the IRE1 $\alpha$  endoribonuclease using kinase inhibitors. *Nat. Chem. Biol.* **2012**, *8*, 982–989.

- (6) Ghosh, R.; Wang, L.; Wang, E. S.; Perera, B. G. K.; Igbaria, A.; Morita, S.; Prado, K.; Thamsen, M.; Caswell, D.; Macias, H.; Weiberth, K. F.; Gliedt, M. J.; Alavi, M. V.; Hari, S. B.; Mitra, A. K.; Bhatarani, B.; Schürer, S. C.; Snapp, E. L.; Gould, D. B.; German, M. S.; Backes, B. J.; Maly, D. J.; Oakes, S. A.; Papa, F. R. Allosteric inhibition of the IRE1 $\alpha$  RNase preserves cell viability and function during endoplasmic reticulum stress. *Cell* **2014**, *158*, 534–548.

- (7) Ranatunga, S.; Tang, C.-H. A.; Kang, C. W.; Kriss, C. L.; Kloppenburg, B. J.; Hu, C.-C. A.; Del Valle, J. R. Synthesis of novel tricyclic chromenone-based inhibitors of IRE-1 RNase activity. *J. Med. Chem.* **2014**, *57*, 4289–4301.

- (8) Xu, C.; Bailly-Maitre, B.; Reed, J. C. Endoplasmic reticulum stress: cell life and death decisions. *J. Clin. Invest.* **2005**, *115*, 2656–2664.

- (9) Kinase profiling was performed using the DiscoverX KINOMEScan platform. For more information, see <http://www.discoverx.com/technology/technology-kinomescan.php>.

- (10) Cee, V. J.; Cheng, A. C.; Romero, K.; Bellon, S.; Mohr, C.; Whittington, D. A.; Bak, A.; Bready, J.; Caenepeel, S.; Coxon, A.; Deak, H. L.; Fretland, J.; Gu, Y.; Hodous, B. L.; Huang, X.; Kim, J. L.; Lin, J.; Long, A. M.; Nguyen, H.; Olivieri, P. R.; Patel, V. F.; Wang, L.; Zhou, Y.; Hughes, P.; Geuns-Meyer, S. Pyridyl-pyrimidine benzimidazole derivatives as potent, selective, and orally bioavailable inhibitors of Tie-2 kinase. *Bioorg. Med. Chem. Lett.* **2009**, *19*, 424–427.

- (11) Payton, M.; Bush, T. L.; Chung, G.; Ziegler, B.; Eden, P.; McElroy, P.; Ross, S.; Cee, V. J.; Deak, H. L.; Hodous, B. L.; Nguyen, H. N.; Olivieri, P. R.; Romero, K.; Schenkel, L. B.; Bak, A.; Stanton, M.; Dussault, I.; Patel, V. F.; Geuns-Meyer, S.; Radinsky, R.; Kendall, R. L. Preclinical evaluation of AMG 900, a novel potent and highly selective pan-aurora kinase inhibitor with activity in taxane-resistant tumor cell lines. *Cancer Res.* **2010**, *70*, 9846–9854.

- (12) The following kinases had POC < 30: LIMK1, PKD2, YSK4, TIE2, and DDR1.

- (13) Lee, K. P. K.; Dey, M.; Neculai, D.; Cao, C.; Dever, T. E.; Sicheriemail, F. Structure of the dual enzyme Ire1 reveals the basis for catalysis and regulation in nonconventional RNA splicing. *Cell* **2008**, *132*, 89–100.

- (14) Korennykh, A. V.; Egea, P. F.; Korostelev, A. A.; Finer-Moore, J.; Stroud, R. M.; Zgnag, C.; Shokat, K. M.; Walter, P. Cofactor-mediated conformational control in the bifunctional kinase/RNase Ire1. *BMC Biol.* **2011**, *9*, 48.

- (15) Ali, M. M. U.; Bagratuni, T.; Davenport, E. L.; Nowak, P. R.; Silva-Santisteban, M. C.; Hardcastle, A.; McAndrews, C.; Rowlands, M. G.; Morgan, G. J.; Aherne, W.; Collins, I.; Davies, F. E.; Pearl, L. H. Structure of the Ire1 autophosphorylation complex and implications for the unfolded protein response. *EMBO J.* **2011**, *30*, 894–905.

- (16) The moderate sensitivity observed for a few cell lines (IC<sub>50</sub>  $\approx$  50-fold greater than XBP1-Luc IC<sub>50</sub>) was not validated in confirmation studies.

- (17) See Supporting Information for assay details.

- (18) A detailed full account of these results will be disclosed separately (manuscript in preparation).